5th International Conference on Experimental Fluid Mechanics ICEFM 2018 Munich
Munich, Germany, July 2-4, 2018

Experimental investigation of the effect of a surface protuberance on the surface heat transfer in a high speed boundary layer

D. P. Ramaswamy[2*], F.F.J Schrijer[1], F. Avallone[1]

[1] Faculty of Aerospace Engineering, Delft University of Technology, The Netherlands

[2] Institute of Aerodynamics, RWTH Aachen University, Germany

[*] d.ramaswamy@aia.rwth-aachen.de

Abstract

An experimental investigation was conducted to study the effect of a surface protuberance on a compressible laminar boundary layer at Mach 6.48 and turbulent boundary layer at Mach 2. The surface heat transfer was studied upstream and downstream of a cylindrical protuberance using quantitative infrared thermography. The influence of the geometry of the cylinder on the surface heat transfer features is clarified for both the laminar and turbulent interactions. Furthermore, boundary layer transition is observed in the laminar interactions by identifying the turbulent wedge in the wake of the protuberance. A series of high and low heat transfer regions are observed in the wake of the protuberance in the turbulent boundary layer, indicating the presence of streamwise vortices.

1 Introduction

An important challenge in the design of high-speed vehicles is aerodynamic heating that is imposed by the flow. While ideally, the external surface should have a smooth geometry, in practice this is not the case and the vehicle typically contains surface discontinuities such as steps, gaps, and other protrusions (Schneider, 2008). These can alter the local flow field and may cause local overheating on the surface (Hung and Clauss, 1980; Hung and Patel, 1984). Hence detailed investigation of the flow behaviour around these protuberances is essential to enable a reliable prediction of the convective heat transfer, which will further aid in the design of a suitable thermal protection system (TPS).

Flow organisation around isolated protuberances have been studied in the past, both computationally and experimentally. In a laminar boundary, the presence of a 3D protuberance may result in a large separation region with multiple spanwise vortices (Baker, 1979; Avallone et al., 2016a) and a heat transfer peak upstream of the protuberance (Kumar et al., 2014; Avallone et al., 2016a). Additionally, the protuberances may act as vortex generators, generating streamwise vortices and eventually forcing transition in some cases (Iyer and Mahesh, 2013; Avallone et al., 2016b). Literature on the interaction of a protuberance with a turbulent boundary layer is focused mainly on the associated protuberance induced shock wave boundary layer interactions (Ozcan and Yuceil, 1992). The unsteady region upstream of the protuberance and the associated aerodynamic heating can be quite pronounced, thus resulting in several investigations in the past. (Evans and Smits, 1996; Yu et al., 2012).

Literature provides insight into the general flow organisation and surface feature evolution around a protuberance. However, in the laminar part, further studies on the upstream separation region and the downstream wake region is essential and the influence of the aspect ratio (AR) of the protuberance was not discussed in great detail. While in the turbulent region, any influence of the protuberance geometry on the heat transfer distribution needs to be investigated, especially in the wake region where a possible high surface shear stress and hence a high heat transfer is expected (Couch, 1969). The present study aims at filling these gaps in literature by performing a parametric study of the effect of surface protuberance in a compressible laminar and turbulent boundary layer using quantitation infrared thermography (QIRT).

2 Experimental Apparatus

2.1 Flow Facility and Wind tunnel models

Two test facilities and wind tunnel models were used to perform measurements. For the laminar interactions, experiments were carried out in the Hypersonic Test facility (HTFD) at the Aerodynamics laboratory of TU Delft (Schrijer and Bannink, 2010). It is a cold hypersonic facility based on the Ludwieg tube concept with a free stream Mach number of 7.5 and a free stream total temperature of 579 K. For this study, experiments were performed at three unit Reynolds numbers - $8 \times 10^6 m^{-1}$, $11 \times 10^6 m^{-1}$ and $14 \times 10^6 m^{-1}$ - and the results corresponding to these three conditions are labelled as Re8, Re11 and Re14 respectively. The laminar boundary layer which develops over a 5^o compression ramp model ($200mm \times 110mm$) was used for this investigation. The wind tunnel model is made of Makrolon®, a polycarbonate material that has favourable thermal properties for the application of infrared thermography. The roughness elements are mounted at $x_r = 60mm$ from the leading edge and along the symmetry axis of the model with a corresponding roughness location based Reynolds number (Re_x) equals 4.8×10^5, 6.6×10^5 and 8.4×10^5. All elements are cylindrical shaped, with a height $H = 2mm$ and diameter equal to $D = 4mm$, $5.7mm$, $8mm$ and $11.2mm$ which will be labelled as D4, D5.7, D8, and D11.2 respectively. The laminar boundary layer thickness (δ) at the location of the protuberance equals $2mm$, $1.7mm$ and $1.5mm$, respectively for increasing values of unit Reynolds number with a corresponding H/δ of 1, 1.17 and 1.33. The experimental conditions and the laminar boundary layer properties are discussed in detail in Avallone et al. (2016b).

For the turbulent interactions, the ST-15 supersonic blow-down wind tunnel was used. The tunnel is operated at Mach 2 at a free stream total pressure of 3.2 bars and a total temperature of $290K$ resulting in a free stream unit Reynolds number of $42.2 \times 10^6 m^{-1}$. The turbulent boundary layer ($\delta = 5.2mm$) at the walls of the wind tunnel is used for this part of the investigation. Roughness elements of three different heights: $H = 6mm$, $8mm$, $10mm$ (labelled as H6, H8 and H10), each with three different diameters: $D = 11.25mm$, $15mm$, $17mm$ (labelled as D1125, D15 and D17) were attached to the walls of the wind tunnel using adhesive tape. Detailed PIV investigations have been carried out in the past in this facility (Giepman et al., 2014), analysing the free stream and boundary layer properties. The incompressible momentum thickness (θ_i) and shape factor (H_i) were determined to be 0.52 and 1.23 respectively, resulting in a Reynolds number based on incompressible momentum thickness $Re_{\theta_i} = 21.8 \times 10^3$.

2.2 Infrared Thermography and Heat Flux Data Reduction

A CEDIP Titanium 530L IR system was used to carry out the quantitative infrared thermographic measurements in both the test facilities. Temperature measurements were made at $218Hz$ and $25Hz$ with a corresponding integration time of $400\mu s$ and $205\mu s$, respectively for the laminar and turbulent interactions for optimal performance. Optical access is provided by a Germanium window, which has a transmissivity of approximately 0.8. Calibration of the camera was carried out using a reference black body and the germanium window was included in the calibration procedure.

Owing to the working nature of the two test facilities used, two different data reduction techniques were followed to obtain the convective heat flux / Stanton number from the temperature measurements. For the measurements conducted in the HTFD, the heat transfer data reduction follows the thin film approach and is based on the 1D semi-infinite model. The 1D unsteady heat conduction equation was solved from which the convective heat transfer was determined using the measured transient surface temperature distribution. Numerical integration of the measured temperature signal was carried out using the Cook and Felderman (1966) approach. Further details regarding the implementation of the data reduction technique can be found in the work of Schrijer (2010). However, the same technique cannot directly be applied to the measurement in the ST-15 facility. For this purpose, a newly developed IR based active heat transfer measurement set-up (Voogt, 2017) was used, based on the heated thin foil approach. It consists of a Printed circuit board (PCB) containing regularly arranged tracks of copper over a 1mm thick FR-4 base material, covering an area of $150mm \times 178mm$. An $8mm$ thick Makrolon®slab was glued and screwed on to the other side of the PCB providing insulation. The assembled test place was then mounted onto a custom built cavity door. The protuberances were glued on to the PCB plate using an adhesive tape with high temperature resistance. The test plate was then heated using an external power supply. Under a steady state condition during wind tunnel operation, the test plate should be in thermal equilibrium with surrounding. The heat flux and hence the convective heat transfer coefficient was then directly computed from the measured temperature under steady

state conditions. More details regarding the test set-up and the data reduction procedure can be found in the work of Voogt (2017).

3 Results

3.1 Protuberance in a laminar boundary layer

The centreline modified Stanton number (C_h) distribution, as seen in Fig 1, provides a first indication of how a protuberance could alter an otherwise smooth laminar boundary layer development. Here, x^* is the stream wise distance scaled with the height of the element, with its origin at the trailing edge of the respective element. The theoretical laminar and turbulent Stanton number, calculated using the reference temperature method (Eckert, 1956) is also shown. A local peak is observed immediately downstream of the element for all diameters and Reynolds numbers. This corresponds to the flow reattachment point which appears to be be invariant with the Reynolds number or the diameter of the element and maintains a constant value of $x^*_R = 3.6 \pm 0.1$. It can also be seen that as the Reynolds number decreases, the flow takes longer to reach a fully turbulent state. For the Re8 case, all the elements failed to attain a turbulent Stanton number within the measurement domain, but are observed to increase towards the reference turbulent level. This effect is more pronounced as the Reynolds number is increased. This is not surprising because the boundary layer thickness decreases with an increase in Reynolds number and hence for the same height, the roughness element is more *effective* at tripping the boundary layer at higher Reynolds number.

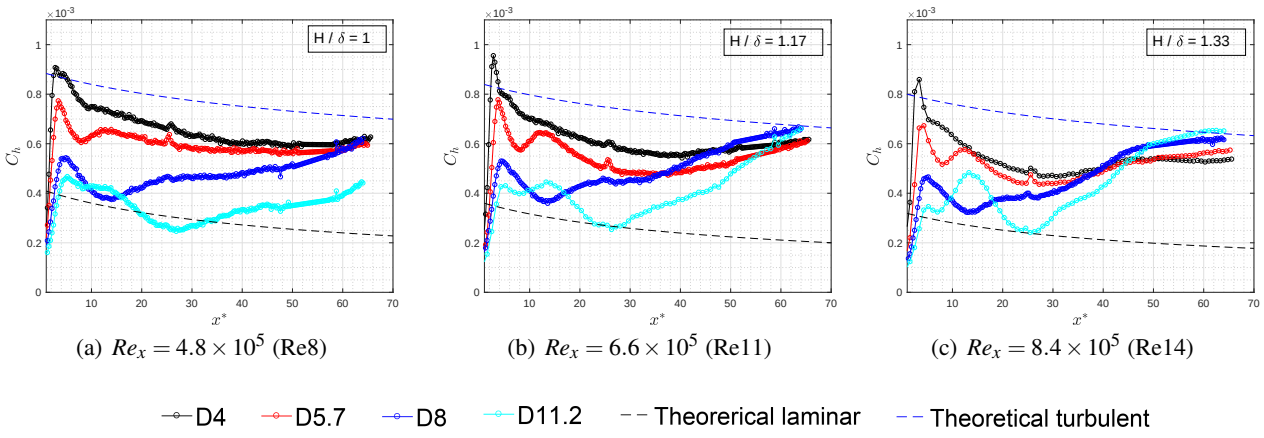

(a) $Re_x = 4.8 \times 10^5$ (Re8) (b) $Re_x = 6.6 \times 10^5$ (Re11) (c) $Re_x = 8.4 \times 10^5$ (Re14)

Figure 1: Centreline Stanton number distribution at for all the roughness geometries. D/H corresponding to elements D4, D5.7, D8 and D11.2 are 2, 2.85, 4 and 5.6 respectively.

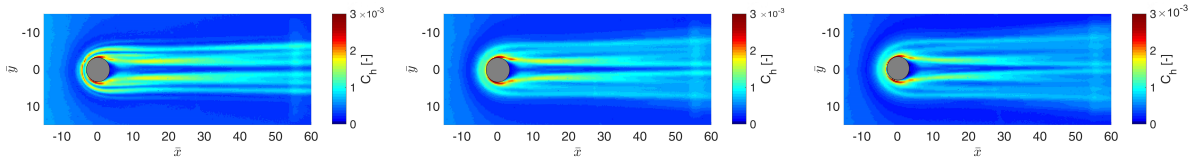

(a) (b) (c)

Figure 2: Modified Stanton Number distribution at (a) $Re_x = 4.8 \times 10^5$, (b) $Re_x = 6.6 \times 10^5$ and (c) $Re_x = 8.4 \times 10^5$ for $D = 11.2mm$ (D/H = 5.6) cylinder

The main advantage of IR thermography is the ability to measure the temperature map and hence the heat transfer map of the entire 2D domain of interest. Fig. 2 shows the modified Stanton number distribution around $D = 11.2mm$ protuberances at three Reynolds numbers. For convenience, the origin of the coordinate

system $(\bar{x}, \bar{y})$ is moved to the centre of the protuberance and scaled with height. A high heat flux region is found upstream of the protuberance for all the Reynolds number cases, which is due to the vortex system in the recirculation region that wraps around the protuberance (Avallone et al., 2016a). A series of high and low heat transfer streaks were observed in the wake of the elements, due to the presence of streamwise vortices causing high and low speed streaks (Iyer and Mahesh, 2013). It is of interest to investigate how strength (expressed in terms of induced heat flux magnitude) the of these vortices correlates to the protuberance geometry.

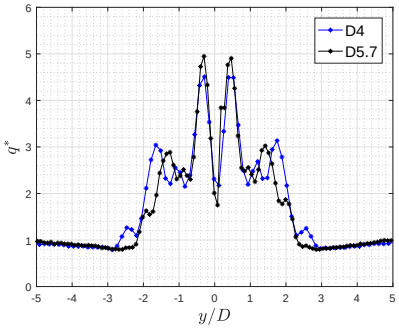

(a) Comparision of $D/H = 2$ (D4) and D/H = 2.85 (D5.7) at $Re_x = 8.4 \times 10^5$

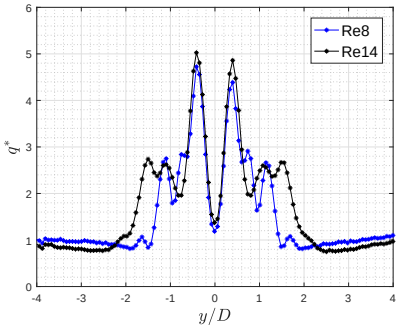

(b) Comparision of $D/H = 4$ at $Re_x = 4.8 \times 10^5$ (Re8) and 8.4×10^5 (Re14)

Figure 3: Spanwise variation of normalised heat flux at $x^* = 10$

Fig. 3(a) shows the span wise variation of heat transfer for two roughness elements at $x^* = 10$. Note that the plotted values are heat flux normalised with respect to the undisturbed laminar heat flux (q^*). The values away from centreline is close to 1, denoting the undisturbed region. The primary heat flux peak, close to the centreline, is observed to increase with an increase in diameter of the element. This was also observed for the other test cases that were investigated (not shown). In general, the normalised heat flux is found to increase with approximately 19.5% when the diameter is increased from $D = 4mm$ to $11.2mm$. The normalised position of these peaks is approximately $y/D = \pm 0.4$. Fig 3(b) shows the spanwise normalised heat flux distribution at the same downstream location for the $D = 8mm$ ($D/H = 4$) cylinder at the lowest and the highest Reynolds number. Similar to the previous case, the location of the primary heat transfer peaks scaled with respect to the diameter of the element. This signifies that the strength and location of the symmetry plane heat transfer peaks and hence the symmetry plane vortices are mainly dependent on the diameter / span of the element. Moreover, there is an 8.5% increase in normalised heat transfer peak magnitude with increase in the Reynolds number.

Observing Fig. 3(b), one can also notice that the wake width for a given element tends to increase with Reynolds number. This was also observed in the 2D heat transfer distribution in Fig. 2. With increase in Reynolds number, a spanwise spreading of the wake occurs forming a *turbulent wedge*. This indicates the onset of boundary layer transition. The origin of the turbulent wedge tends to move upstream with increase in flow unit Reynolds number. Since the height of all the roughness elements in the laminar interaction is constant ($H = 2mm$), the onset of transition can hence be said to more upstream with increase in roughness height based Reynolds number (Re_H). A similar observation was also made by Ye et al. (2016).

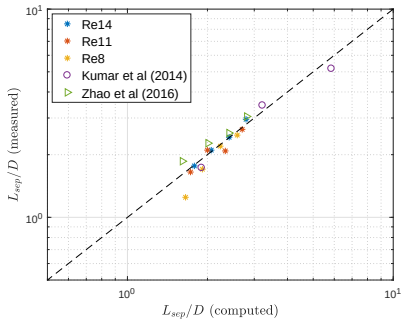

Figure 4: Empirical correlation for L_{sep}

Moving upstream, a heat transfer peak is observed due to the presence of span wise vortices in the recirculation region. The upstream separation length (L_{sep}) is calculated from the centreline heat transfer distribution as the distance between the leading edge of the protuberance and the point where the Stanton number distribution starts to deviate from the laminar profile. An empirical correlation based on the work of Hung and

Clauss (1980) for short protuberances was developed:

$$\frac{L_{sep}}{D} = 3.5\left(\frac{H}{\delta}\right)^{0.7}\left(\frac{D}{\delta}\right)^{-0.435} \tag{1}$$

Fig 4 shows the upstream separation length measured and predicted by Eqn. 1, showing satisfactory agreement. The upstream separation length obtained from recent literature (Kumar et al., 2014; Zhao et al., 2016) is also plotted, providing further confidence. This correlation highlights the influence of diameter of the protuberance on the separation upstream, in contrast to the studies carried out earlier where the influence of height was only considered (Kumar et al., 2014).

3.2 Protuberance in a turbulent boundary layer

Similar to the laminar case, the 2D heat flux distribution around a circular protuberance in a turbulent boundary layer will be discussed, assisted by sectional plots in the streamwise and spanwise directions. Fig. 5 shows the distribution of centreline normalised convective heat transfer coefficient ($h^* = h_{test}/h_{turb}$) in the wake of the cylinder. The heat transfer in the wake of the cylinder is nearly 1.5 - 2 times the local reference turbulent heat transfer and tends to increase with increase in H/δ of the cylinder. A local peak corresponding to the reattachment point is observed immediately downstream of the element for all the cases and similar to the laminar case, its location scaled with the height of the cylinder. For all the geometries reported here, the scaled reattachment location remained fairly constant with $x^*_R = 1.47 \pm 0.2$. The heat transfer profiles tend to portray a downward slope towards the end of the measurement domain, indicating the a recovery of the boundary layer towards turbulent conditions..

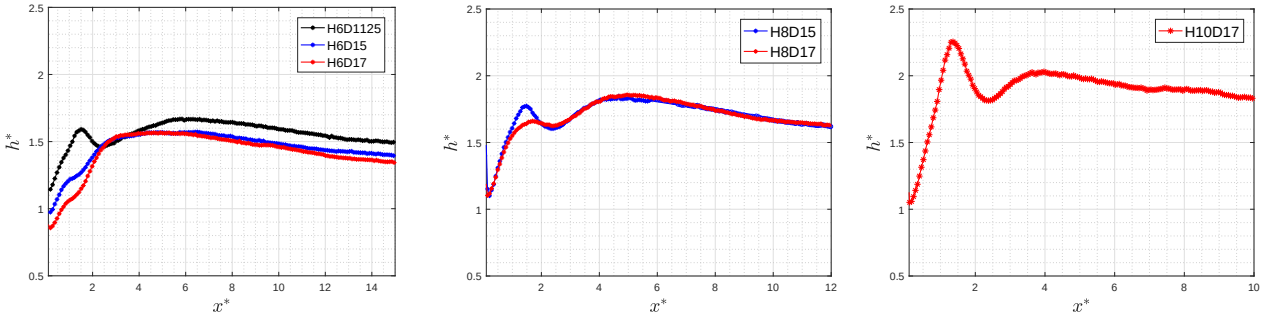

(a) $H/\delta = 1.15$ (b) $H/\delta = 1.53$ (c) $H/\delta = 1.92$

Figure 5: Centreline heat transfer distribution in the wake region

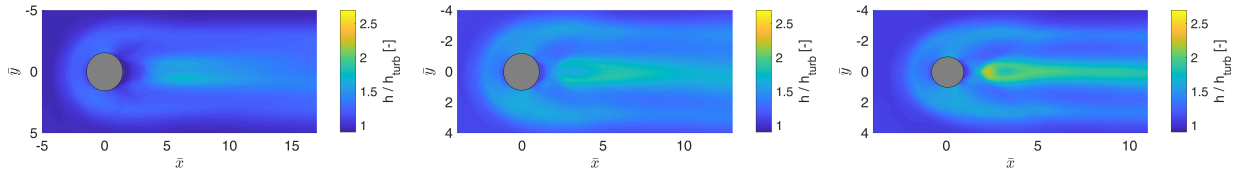

(a) $H/\delta = 1.15$ (b) $H/\delta = 1.53$ (c) $H/\delta = 1.92$

Figure 6: 2D heat transfer distribution for $D = 17mm$ cylinder ($D/\delta = 3.27$) at different heights

The 2D heat transfer distribution of the $D = 17mm$ cylinder at all the three heights is shown in Fig. 6. A high heat transfer region can be found upstream of the cylinder due to the presence of a recirculation region. The high heat transfer region is observed to wrap around the protuberance and extends downstream, similar to what was observed in the laminar case. Downstream of the element, the wake is characterised by a low and high heat transfer streaks. The sustained streaks point to the possible existence of streamwise vortices similar to those observed in the laminar case. The wake width is seen to remain constant till the end

of the measurement domain. Fig. 7 shows the span wise heat transfer distribution, plotted at $x^* = 7.5$ for the $D = 17mm$ cylinder. where the wake width is observed to increase with increase in height of the element.

In addition to QIRT measurements, high speed schlieren images were also captured for all the geometries, upstream of the protuberance. The images were acquired at 62.5kHz with an exposure time equal to $1.7\mu s$. The resulting frames are processed to extract the time resolved position of the separation shock at each pixel in the wall normal direction using the Sobel edge detection algorithm. A linear curve fit is then applied to the shock position to estimate the point at which the shock would hit the wall, providing the upstream separation distance (L_{sep}). The probability density function of the upstream separation distance (see Fig. 8(a)) shows a near normal distribution. Also the peak probabilities are seen to decrease with increase in height. The mean separation length estimated from Schlieren images, QIRT and oil flow measurement are shown in Fig. 8(b). There is a good match in upstream separation length estimates, measured with various techniques and it is within the measurement uncertainty. An increase in upstream separation distance with the height of the protuberance is seen. For all height considered here, L_{sep} was within 2 cylinder diameters. The standard deviation of the shock oscillation portrayed as error bars in Fig. 8(b), is a good measure to study the unsteadiness of the oscillation separation shock. The standard deviation is also observed to increase with increase in height of the cylinder, varying between 0.09 to 0.156 cylinder diameters.

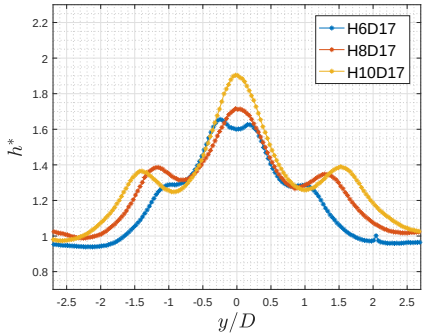

Figure 7: Spanwise distribution of normalised heat transfer coeffcient at $x^* = 7.5$

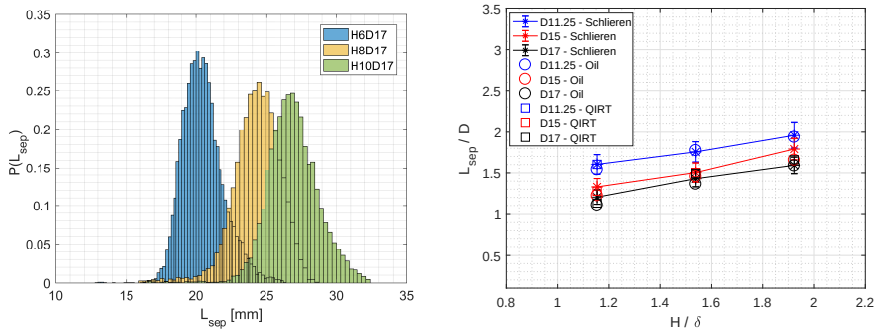

(a) PDF of the upstream separation length

(b) Mean separation

Figure 8: Statistic of the separation length.

4 Conclusion

In the present study, the heat transfer around cylindrical protuberances in a compressible laminar and turbulent boundary layer is studied using quantitative infrared thermography. The surface heat transfer features are studied for different geometrical and flow conditions. The presence of a protuberance causes a series of low and high heat transfer streaks in the wake region. The flow reattachment downstream induces a local heat transfer peak, the location of which scaled with the height of the protuberance in both a laminar and a turbulent boundary layer interactions. In the laminar boundary layer, the strength and the location of the primary peaks caused due to the symmetry plane counter-rotating vortices depend mainly on the diameter of the protuberance. The turbulent wedge, and hence the flow transition point was seen to move upstream with an increase in roughness height based Reynolds number. The predictions of upstream separation length by the empirical correlation that was formulated, shows good with the current dataset, along with recent literature. On the contrary, probability density function of upstream separation estimated in turbulent interaction case portrays that both the mean and standard deviation increases with increase in height of the cylinder.

References

Avallone F, Ragni D, Schrijer FFJ, Scarano F, and Cardone G (2016a) Study of a Supercritical Roughness Element in a Hypersonic Laminar Boundary Layer. *AIAA Journal* 54:1892–1900

Avallone F, Schrijer FFJ, and Cardone G (2016b) Infrared thermography of transition due to isolated roughness elements in hypersonic flows. *Physics of Fluids* 28:024106

Baker CJ (1979) The laminar horseshoe vortex. *Journal of Fluid Mechanics* 95:347

Cook WJ and Felderman EJ (1966) Reduction of data from thin-film heat-transfer gages - a concise numerical technique. *AIAA Journal* 4:561–562

Couch LM (1969) Flow field measurements on flat plate with attached protuberances in supersonic turbulent boundary layer. Technical Report NASA-TN-D-5297. NASA Langley Research Center

Eckert E (1956) Engineering relations for heat transfer and friction in high-velocity laminar and turbulent boundary-layer flow over surfaces with constant pressure and temperature. *Transactions of the Americal Soceity of Mechanical Engineers* 78:1273–1283

Evans TT and Smits AJ (1996) Measurements of the mean heat transfer in a shock wave-turbulent boundary layer interaction. *Experimental Thermal and Fluid Science* 12:87–97

Giepman RHM, Schrijer FFJ, and van Oudheusden BW (2014) Flow control of an oblique shock wave reflection with micro-ramp vortex generators: Effects of location and size. *Physics of Fluids* 26:066101

Hung F and Clauss J (1980) Three-dimensional protuberance interference heating in high speed flow. in *18th Aerospace Sciences Meeting*. American Institute of Aeronautics and Astronautics

Hung F and Patel D (1984) Protuberance interference heating in high-speed flow. in *19th Thermophysics Conference*. American Institute of Aeronautics and Astronautics

Iyer PS and Mahesh K (2013) High-speed boundary-layer transition induced by a discrete roughness element. *Journal of Fluid Mechanics* 729:524–562

Kumar CS, Singh T, and Reddy KPJ (2014) Investigation of the separated region ahead of three-dimensional protuberances on plates and cones in hypersonic flows with laminar boundary layers. *Physics of Fluids* 26

Ozcan O and Yuceil BK (1992) Cylinder-induced shock-wave boundary-layer interaction. *AIAA Journal* 30:1130–1132

Schneider S (2008) Effects of Roughness on Hypersonic Boundary-Layer Transition. *Journal of Spacecraft and Rockets* 45:193–209

Schrijer FFJ (2010) *Experimental investigation of re-entry aerodynamic phenomena - Development of non-intrusive Flow diagnostics in a Ludwieg tube*. Phd thesis. the Netherlands

Schrijer FFJ and Bannink WJ (2010) Description and flow assessment of the delft hypersonic ludwieg tube. *Journal of Spacecraft and Rockets* 47:125–133

Voogt N (2017) *Investigation on supersonic, large wall roughness elements using QIRT and PIV.*. Master's thesis. TU Delft. the Netherlands

Ye Q, Schrijer FFJ, and Scarano F (2016) Infrared Thermography Investigation of Transitional flow over Isolated Roughness at high speeds. in *51st 3AF International Conference on Applied Aerodynamics*

Yu MS, Song J, Bae JC, and Cho HH (2012) Heat transfer by shock-wave/boundary layer interaction on a flat surface with a mounted cylinder. *International Journal of Heat and Mass Transfer* 55:1764–1772

Zhao Y, Liu W, Xu D, Gang D, and Yi S (2016) A combined experimental and numerical investigation of roughness induced supersonic boundary layer transition. *Acta Astronautica* 118:199–209